Optical forces on metallic nanoparticles induced by a photonic nanojet

Xudong Cui [*1], Daniel Erni [1], Christian Hafner [2]

[1] *General and Theoretical Electrical Engineering (ATE), Faculty of Engineering, University of Duisburg-Essen, D-47057, Duisburg, Germany*
[2] *Laboratory for Electromagnetic Fields and Microwave Electronics, ETH Zurich, CH-8092, Zurich, Switzerland*

[*] *Corresponding author: xudong.cui@uni-due.de*

Abstract: We investigate the optical forces acting on a metallic nanoparticle when the nanoparticle is introduced within a photonic nanojet (PNJ). Optical forces at resonance and off-resonance conditions of the microcylinder or nanoparticle are investigated. Under proper polarization conditions, the whispering gallery mode can be excited in the microcylinder, even at off resonance provided that scattering from the nanoparticle is strong enough. The optical forces are enhanced at resonance either of the single microcylinder or of the nanoparticle with respect to the forces under off-resonant illuminations. We found that the optical forces acting on the nanoparticle depend strongly on the dielectric permittivity of the nanoparticle, as well as on the intensity and the beam width of the PNJ. Hence, metallic sub-wavelength nanoparticle can be efficiently trapped by PNJs. Furthermore, the PNJ's attractive force can be simply changed to a repulsive force by varying the polarization of the incident beam. The changed sign of the force is related to the particle's polarizability and the excitation of localized surface plasmons in the nanoparticle.

OCIS codes: (290.0290) Scattering; (020.7010) Trapping; (240.6680) Surface plasmons.

References and links

1. Z. Chen, A. Taflove, and V. Backman, "Photonic nanojet enhancement of backscattering of light by nanoparticles: a potential novel visible-light ultramicroscopy technique, " Opt. Express **12**, 1214-1220 (2004).
2. V. Itagi and W. A. Challener, "Optics of photonic nanojets," J. Opt. Soc. Am. A **22**, 2847-2858 (2005).
3. A. Heifetz, J. J. Simpson, S. C. Kong, A. Taflove, and V. Backman, "Subdiffraction optical resolution of a gold nanosphere located within the nanojet of a Mie-resonant dielectric microsphere," Opt. Express **15**, 17334-17342 (2007).
4. X. Li, Z. Chen, A. Taflove, and V. Backman, "Optical analysis of nanoparticles via enhanced backscattering facilitated by 3-D photonic nanojets," Opt. Express **13**, 526-533 (2005).
5. A. Heifetz, K. Huang, A. V. Sahakian, X. Li, A. Taflove, and V. Backman, "Experimental confirmation of backscattering enhancement induced by a photonic jet," Appl. Phys. Lett. **89**, 221118 (2006).
6. V. Sandoghdar, E. Klotzsch, V. Jacobsen, A. Renn, U. Hakanson, M. Agio, I. Gerhardt, J. Seelig, and G. Wrigge, "Optical detection of very small nonfluorescent nanoparticles," CHIMIA **60**, 761-764 (2006).
7. Ch. Hafner, *Post-Modern Electromagnetics* (Wiley, Chichester, 1999).
8. http://max-1.ethz.ch.
9. P. C. Chaumet and M. Nieto-Vesperinas, "Coupled dipole method determination of the electromagnetic force on a particle over a flat dielectric substrate," Phys. Rev. B. **61**, 14119-14127 (2000).
10. C. Rockstuhl and H. P. Herzig, "Wavelength dependent optical force on elliptical silver cylinders at plasmon resonance," Opt. Lett. **29**, 2181-2183 (2004).
11. V. Wong and M. A. Ratner, "Size dependence of gradient and nongradient optical forces in silver nanoparticles," J. Opt. Soc. Am. B **24**, 106-112 (2007).
12. A. S. Zelenina, R. Quidant, and M. Nieto-Vesperinas, "Enhanced optical forces between coupled resonant metal nanoparticles," Opt. Lett. **32**, 1156-1158 (2007).
13. P. Johnson and R. Christy, "Optical constants of noble metals," Phys. Rev. B **6**, 4730-4739 (1972).

#98001 - $15.00 USD Received 30 Jun 2008; revised 14 Aug 2008; accepted 15 Aug 2008; published 19 Aug 2008

14. J. R. Arias-Gonzalez and M. Nieto-Vesperinas, "Optical force on small particles: attractive and repulsive nature and plasmon-resonance conditions," J. Opt. Soc. Am. A **20**, 1201-1209 (2003).

1. Introduction

Photonic nanojets (PNJs) are obtained on the shadow-side of a dielectric microcylinder under plane wave illumination [1] when the refractive index is tuned in such a way that an emerging focus is located on the surface of the cylinder in order to exploit the large spatial resolution of evanescent harmonics. Due to the small waist and divergence, PNJs are attractive for ultramicroscopy techniques for imaging and for detection applications [1]. Numerical and experimental studies [1-3] show that backscattering can be enhanced by several orders of magnitude by placing nanoparticles within the PNJs, where the perturbation of the backscattering shows a dependence on the third power of the particle's size [3, 4, 5]. As a result, nanoparticles as small as 10 nm can be detected when they are approaching a properly designed microcylinder [3, 4]. Note that the detection methods based on particle scattering are usually limited by the weak scattering intensities of small particles [6], because the scattering cross section of a particle with radius R being much smaller than the wavelength λ varies according to R^6. Therefore, it would be crucial to reduce this size dependence to improve the detection sensitivity when far-field based detection techniques are employed. The use of PNJs might offer both, an enhanced spatial resolution and a circumvention of the scattering cross section's crucial size dependence.

Because of their nonresonant properties, PNJs exist over a wide parameter range with respect to the size and the material properties of the dielectric microcylinder. The extent and the width of the PNJ can be efficiently controlled and even tuned close to the diffraction limit of the incident light, when the shape and the refractive index of the microcylinder are properly chosen [2]. Therefore, it is reasonable to treat the PNJ as an adjustable light source supporting high intensities at sub-aperture size. The nanoparticle under detection can then be manipulated by the optically induced forces stemming from the large intensity gradients of PNJs. Motivated by the attractive features of the PNJs, we have carefully analyzed the optical forces induced from the PNJs, which are acting on the nanoparticles at resonant and non resonant conditions of the microcylinder-nanoparticle system. We found that the optical forces are enhanced near the resonance of the microcylinder as well as of the nanoparticles and, moreover, that the optical forces induced by the PNJs exerting on the nanoparticle strongly depend on the dielectric permittivity of the nanoparticle. We also show that attractive forces can be converted into repulsive forces exerting simply by varying the polarization of the incident beam.

2. Modeling and simulation considerations

Since PNJ emission exists for a wide range of the dielectric microcylinder sizes, one can select a proper microcylinder to generate a PNJ with a desired focal area. In general, the Full-Width at Half Maximum (FWHM) of the PNJ decreases and the field enhancement within the PNJ emission increases when the size of the microcylinder is reduced. In addition the focal area also tends to be confined more closely to the surface for smaller microcylinder sizes [1]. Here, a PNJ with a small FWHM is chosen in our study. It is worth noting that the size of the microcylinder extends in most cases towards several micrometers and is therefore always much larger than the operation wavelength. In order to obtain highly accurate results for the PNJ calculations, a proper choice with respect to the numerical method is mandatory. For domain methods such as Finite-Difference Time-Domain (FDTD) [1], very fine meshes are required to get reliable results since the structure size is much larger than the incident wavelength. In addition, time-domain methods are disadvantageous when strong dispersive materials like metals at optical frequencies are involved. A powerful alternative is offered by the boundary methods in the frequency domain, where the multiple multipole program (MMP) [7-8] fulfills all the aforementioned requirements. The semi-analytical MMP method is essentially an extension of the analytical Mie theory, which is well known for its accurate

#98001 - $15.00 USD Received 30 Jun 2008; revised 14 Aug 2008; accepted 15 Aug 2008; published 19 Aug 2008

approximations in optical particle analysis. In order to reduce the complexity of the overall setting and without loss of generality we have carried out all the simulations along a two dimensional (2D) analysis. The electromagnetic field inside a 2D particle is therefore expressed by the Mie approximation using Bessel expansions as following [7]

$$E_{zi}(r,\varphi) = A_{i0}^{E} J_0(kr) + \sum_{n=1}^{N_i} A_{in}^{E} J_n(kr)\cos(n\varphi) + B_{in}^{E} J_n(kr)\sin(n\varphi) \quad (1)$$

$$H_{zi}(r,\varphi) = A_{i0}^{H} J_0(kr) + \sum_{n=1}^{N_i} A_{in}^{H} J_n(kr)\cos(n\varphi) + B_{in}^{H} J_n(kr)\sin(n\varphi) \quad (2),$$

where *A* and *B* denote the corresponding expansion coefficients and *J(.)* is Bessel function. Note that polar coordinates are used here. The transverse field components are retrieved from the longitudinal ones using corresponding differential operators where each consists of linear combinations of the gradients of (1) and (2) (cf. e.g. [7]). The expansions for the scattered field outside a 2D particle are very similar to (1) and (2),

$$E_{zi}(r,\varphi) = a_{i0}^{E} H_0(kr) + \sum_{n=1}^{N_i} a_{in}^{E} H_n(kr)\cos(n\varphi) + a_{in}^{E} H_n(kr)\sin(n\varphi) \quad (3)$$

$$H_{zi}(r,\varphi) = a_{i0}^{H} H_0(kr) + \sum_{n=1}^{N_i} a_{in}^{H} H_n(kr)\cos(n\varphi) + b_{in}^{H} H_n(kr)\sin(n\varphi) \quad (4)$$

.

Here, the Bessel functions *J(.)* are simply replaced by Hankel functions *H(.)*. These functions describe either incoming or outgoing electromagnetic waves, depending on the kind of the Hankel function and the corresponding sign of the wave number *k*. The arguments of the Bessel and Hankel functions are either real or imaginary when material losses are absent. Otherwise, *k* becomes complex. Note that in 2D analysis only a 1D boundary needs to be discretized leading to short computation times and small memory requirements. In MMP, the parameters *A*, *B*, *a*, and *b* are computed while implying the continuity conditions for the electromagnetic field components on the particle's surface, where potential matching errors are minimized in a least-square sense [7]. It should be noted that the transition from 2D to 3D expansions is simple. Instead of polar coordinates (r, φ), spherical coordinates (r, φ, θ) are used in 3D case. From the radial components one may derive the φ and θ components-essentially as in 2D from linear combinations of the gradients of the radial components. For details, see [7].

The optical forces are calculated according to the Maxwell stress tensor [9]. For a particle embedded in an isotropic medium, the exerted, time-averaged force is calculated according to

$$\boldsymbol{F} = \iint_S \left[\tfrac{\varepsilon}{2} \cdot \mathrm{Re}\left\{ (\boldsymbol{E}\cdot\boldsymbol{n})\,\boldsymbol{E}^* \right\} - \tfrac{\varepsilon}{4} \cdot \left(\boldsymbol{E}\cdot\boldsymbol{E}^* \right)\boldsymbol{n} + \tfrac{\mu}{2} \cdot \mathrm{Re}\left\{ (\boldsymbol{H}\cdot\boldsymbol{n})\,\boldsymbol{n}^* \right\} - \tfrac{\mu}{4} \cdot \left(\boldsymbol{H}\cdot\boldsymbol{H}^* \right)\boldsymbol{n} \right] \cdot d\boldsymbol{A} \quad (5)$$

where *S* stands for the boundary (i.e. the circumference) of the particle and *n* denotes the unit vector normal to the surface, Re{.} is the real part, * assigns the complex conjugate, ε and μ are the permittivity and the permeability of the particle, and $\boldsymbol{E}$ and $\boldsymbol{H}$ displays the total electric and magnetic fields, respectively. In the framework of MMP the total electric and magnetic fields in the vicinity of the particle can then be computed from Eqs. (1)-(4). The optically induced forces on the particle are then obtained from Eq. (5). Typically, Eq. (5) represents a surface integral of the area density of the force field, where the latter is obtained from the Maxwell stress tensor at the particle's surface. It should be noted that the force calculated by Eq. (5) is a time-averaged quantity since only average forces are effective in the time scales of the resulting particle movement [10, 11, 12]. Without loss of generality, the total optical force exerted on the nanoparticle can be decomposed into two components with respect to the

#98001 - $15.00 USD Received 30 Jun 2008; revised 14 Aug 2008; accepted 15 Aug 2008; published 19 Aug 2008

nanojet's extent: the lateral force and the axial force, which are equivalent to the often-used concepts of the scattering force and gradient force in optical trappings [11]. The lateral force acts to pull the particle in alignment with the center of the beam while the axial force tends to push/pull the particle along its optical axis.

3. Results and discussion

The structure under consideration is shown in Fig. 1. Here, the radius of the microcylinder is $r_1 = 1$ μm and the refractive index of the microcylinder is 1.59. As displayed in Fig. 1 a plane wave at an initial wavelength of 400 nm is incident from the left and impinges on the microcylinder. All structures are embedded in air and the structural parameters of the PNJ are adapted from [1] for comparison reasons. A silver metallic nanoparticle [13] is exposed to the PNJ. The separation between the microcylinder and the nanoparticle is indicated by *l*, which corresponds to the distance between the outer surfaces of the microcylinder and particle.

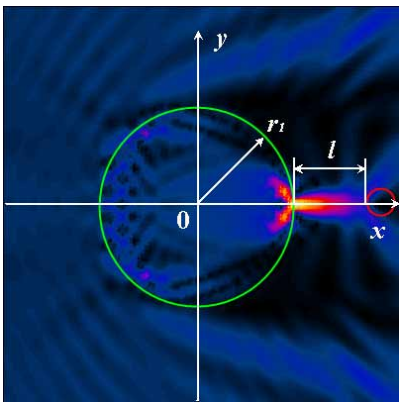

Fig. 1. Schematic drawing of the overall structure. The separation between the dielectric microcylinder and the particle is indicated by the distance *l*. The picture shows the time-averaged Poynting vector field for a *Ez*-polarized plane wave excitation from the left at an operation wavelength of 400 nm. The emergent PNJ is clearly observed.

Figure 2(a) shows a time evolution of the Poynting vector field when the metallic nanoparticle intersects the PNJ while traveling along the *y*-direction for an *Ez*-polarized plane wave illumination from the left at $\lambda = 400$ nm. The metallic nanoparticle has a diameter of 120 nm and the separation distance *l* between the microcylinder and the nanoparticle along the *x*-direction amounts to 40 nm. This position does not correspond to the PNJ's focal point where the intensity is maximal. We will show later, that the strongest forces will emerge at a slightly different location where the gradient of the local field intensity achieves its maximum. Along this evolution a most remarkable feature is observed in Fig. 2(a): When the nanoparticle approaches the PNJ, a whispering gallery mode (WGM) is instantly generated in the microcylinder. WGMs usually denote a highly resonant state where light is confined near the surface of a disk or a spherical object by total internal reflection and is returned in phase after the revolution along the perimeter. Since the microcylinder is off-resonance at the operation wavelength of 400 nm, the generation of a WGM in this compound structure likely arises from the strong reflection induced by the nanoparticle. It is due to the highly localized nature of the light field in PNJ that the scattering contributions stemming from such distinct back-reflection channel are directly provided to the resonance condition of the corresponding WGM. Intensive numerical investigations have revealed that when the particle size reduces to e.g. 20 nm, it becomes impossible to excite WGMs for separation distances larger than $l = 40$ nm, due to the particle's small scattering intensity. The resonances show strong polarization dependence: we could not find a WGM for *H*-polarization in the same configuration as depicted in Fig. 2(a), even for metallic nanoparticles with diameters as large as 120 nm, which almost touch the microcylinder. The time evolution provided in Fig. 2(a)

#98001 - $15.00 USD Received 30 Jun 2008; revised 14 Aug 2008; accepted 15 Aug 2008; published 19 Aug 2008

uncovers another remarkable fact. It turns out that the field intensity (detected at a distance x = 3μm on the x axis shown in Fig.1a) reaches its maximum for a collinear arrangement of both the particle and the nanojet, which is equivalent to placing the centers of the microcylinder and the nanoparticle on the x-axis. This can help to determine the exact location of the nanoparticle according to the above-obtained intensity-distance relation.

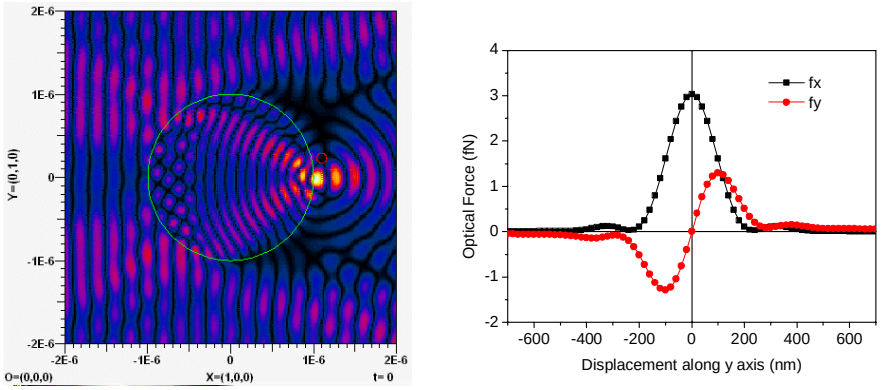

(a) (b)

Fig. 2. (a) (Media 1) Evolution of the Poynting vector field when a metallic nanoparticle (indicated by the small red circle) is crossing the PNJ generated by the dielectric microcylinder (indicated by the green circle). The silver nanoparticle has a diameter of 120 nm and is moving downwards along the y-direction. The overall structure is excited by an Ez-polarized plane wave from the left having an operation wavelength of 400 nm. The horizontal separation l between the particle and the microcylinder is 40 nm. (b) Components of the optically induced force exerted on the nanoparticle while performing the aforementioned transit through the PNJ.

The optical force exerted on the nanoparticle under E-polarization is shown in Fig. 2(b). As indicated in the figure, the axial force f_x represents a strong repulsive force while the nanoparticle is approaching the nanojet. The lateral force f_y changes its sign on the two sides of nanojet and becomes zero in the center, i.e. on the x-axis. The amplitude of f_y reaches two extremes along the y-direction, each being 100 nm apart from the nanojet center.

The optical force acting on the particle is strongly affected by the size of the particle itself, as well as by the separation between the particle and the nanojet. To further investigate the aforementioned influence of both, the particle size and the separation distance l, we calculate the optical forces acting on a smaller metallic nanoparticle at different separation distance l under the illumination of an E-polarized plane wave at a wavelength of 400 nm. The results are shown in Fig. 3, where Fig. 3(a) depicts the case when the separation distance l is 300 nm and the particle diameter is 20 nm. Here, the separation distance l is selected to be larger than in Fig. 2(a) but still smaller than the decay length of the intensity in the PNJ. We select this distance in order to explore the interaction distance of the force, since the particle is still within the PNJ but far away from its center. Although the axial force f_x in Fig. 3(a) displays as a repulsive behavior, its amplitude is much weaker than the lateral force f_y when the particle is leaving the PNJ (at ±100 nm in y-direction). The axial force f_x shown in Fig. 3(a) is enhanced by a factor of 60 compared to the axial force f_x shown in Fig. 2(b). When further reducing the separation distance l to 10 nm, the axial force f_x decreases whereas the lateral force f_y increases as depicted in Fig. 3(b). Typically, there exists a characteristic range of particle sizes, where the repulsive force can be converted to an attractive force, provided that the size of the particle is properly selected in the configuration of Fig. 2(a) (i.e., a small particle with diameter 20 nm). In addition, with decreasing particle size and separation distance, the lateral force f_y increases while the axial force f_x remains constant, providing an opportunity to move the metallic nanoparticle on a surface by lateral forces only. Note that

#98001 - $15.00 USD Received 30 Jun 2008; revised 14 Aug 2008; accepted 15 Aug 2008; published 19 Aug 2008

both forces f_x and f_y exhibit a kind of short-range interaction, which provides highly confined areas of influence for particle manipulation.

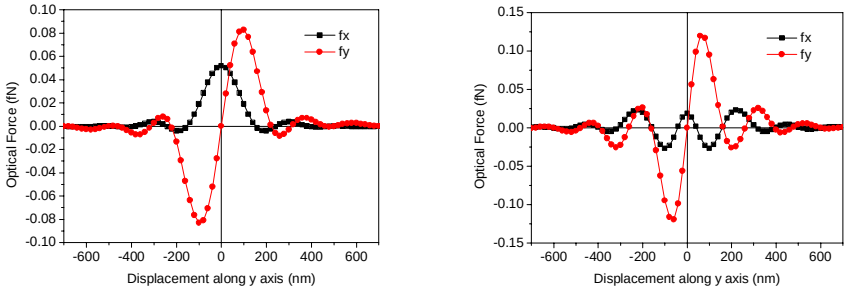

Fig. 3. (a) Calculation of the optically induced force on the silver particle (diameter 20 nm) when the nanoparticle is moving downwards along the *y*-direction with a horizontal separation $l = 300$ nm for the configuration depicted in Fig. 2(a). (b) The same setting but now with a 10 nm separation distance. In both cases the structure is excited by a plane wave with *E*-polarization from the left at an operation wavelength of 400 nm.

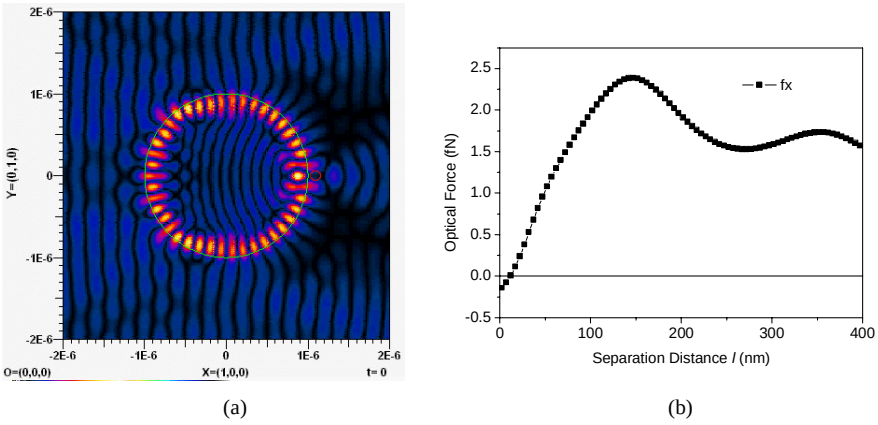

Fig. 4. (a) (Media 2) Distribution of the electric field (Ez) within the microcylinder-nanoparticle system when the metallic nanoparticle (diameter 120 nm) is moving along the *x*-axis. (b) Evolution of the *x*-component of the resulting optically induced force for increasing separation distances. The overall structure is excited by an *Ez*-polarized plane wave from the left at an operation wavelength of 400 nm.

Special attention is paid to the investigation of f_x since the axial forces can help to determine the relative location of the particle to the PNJ. A straightforward way for this purpose is to let the particle move towards the nanojet while monitoring the axial force f_x along the *x*-axis. In order to provide an intuitive picture for the field evolution in this case, an animation is given in Fig. 4(a), and the corresponding optical forces are calculated and displayed in Fig. 4(b) as a function of the separation distance *l*. The axial forces f_x show a repulsive nature for larger separation distances, i.e., when $l > 11$ nm. Attractive forces are only observed for separation distances less than 11 nm. An equilibrium position is therefore found at $l = 11$ nm where the total force (f_x and f_y) is zero. The repulsive force reaches several local maxima and shows a quasi-periodic behavior for the silver particle with diameter 120 nm. For instance, two local maxima appear at the separation distances $l = 145$ nm and $l = 350$ nm. This further indicates that the force amplitude is modulated as a function of *l*, even for large separations and that the amplitude decreases (not monotonically) with the increasing separation distance *l*.

#98001 - $15.00 USD Received 30 Jun 2008; revised 14 Aug 2008; accepted 15 Aug 2008; published 19 Aug 2008

Next, we investigate the optical forces under different illumination wavelengths (at off-resonances either of the mircocylinder or of the particle). The configuration is the same as used in Fig. 4(a) but with a reduced particle diameter of 20 nm. Figure 5 displays the evolution of the axial force as a function of the separation distances. The optical force increases with increasing wavelength for both components f_x and f_y (f_y not shown here), showing strong frequency dependence. The maxima of the optical forces slightly depend on the wavelength. An equilibrium position (where the total force is zero) is found only for sufficiently short wavelengths. No attractive forces are found at the wavelengths 700 nm and 1550 nm, indicating that the PNJ is not optimal with respect to the desired intensity gradients for trapping the nanoparticle at such wavelengths. Figure 5 also indicates that the optical force is strong when the particle scattering becomes large. Besides the strong scattering contribution, large optical forces can be expected also at long wavelengths due to the small metallic losses in the particles.

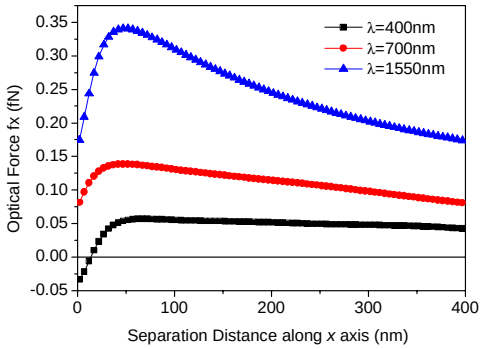

Fig. 5. Evolution of the optically induced force (*x*-component) on the metallic nanoparticle for the case where the particle is moving along *x*-axis. The particle's diameter is 20 nm. The overall structure is illuminated by a *Hz*-polarized plane wave for three different operating wavelengths.

Since the calculations are carried out in two dimensions, our PNJ analysis also supports polarization dependence, namely the illumination under *E*-polarization as well as under *H*-polarization. However, the scattering properties of the microcylinder-particle system under *H*-polarization are different compared to the case of *E*-polarization. The field intensities for both polarizations are shown in Fig. 6(a). They were computed for a distance of 2.1 μm apart from the surface of the microcylinder. As one can see from Fig. 6(a), the intensity perturbation caused by the presence of the nanoparticle is much stronger for *H*-polarization than for *E*-polarization.

The optical force under *H*-polarization displays a nearly opposite behavior compared to the optical force under *E*-polarization [Fig. 2(b)]: the *x* component changes the sign, while the *y* component changes the sign when the displacement between the particle and PNJ is larger, i.e., when the displacement along *y* axis is larger than 100nm as shown in Fig. 6(b). The total optical force is attractive when the nanoparticle is approaching the PNJ. The sign change in the force may be explained by the specific polarizability of the particle and with the generation of a surface plasmon. Nevertheless, the amplitude of the optical force under *E*-polarization [Fig. 2(b)] is almost two times larger than for *H*-polarization [Fig. 6(b)] when the particle is located on the *x*-axis. This is understandable since the scattering intensity of the metallic particle under *H*-polarization is less than that of the metallic particle for *E*-polarization, both for a wavelength of 400 nm, whilst the optical force exerted on the metallic nanoparticle is found to be proportional to the scattering intensity [14]. Interestingly, a dip was found at $y = 0$ (i.e. on the *x*-axis) in the lateral force profile of f_x as shown in Fig. 6(b). The force doesn't reach maximum and it differs from the case of *E*-polarization when the particle

#98001 - $15.00 USD Received 30 Jun 2008; revised 14 Aug 2008; accepted 15 Aug 2008; published 19 Aug 2008

and the PNJ are collinear. We attribute this to the different scattering properties with respect to the polarization conditions and the weaker variation of the local field.

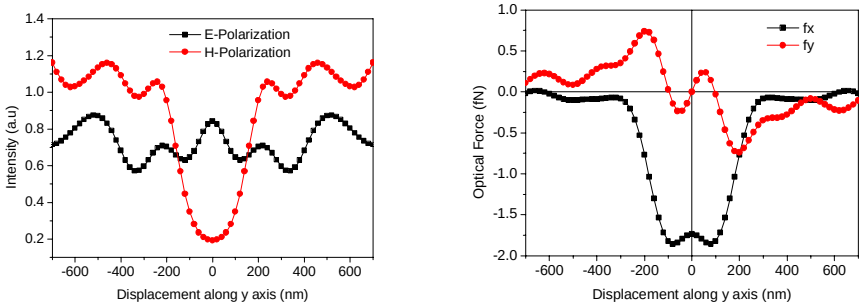

(a) (b)

Fig. 6. (a) Computed lateral field intensity profiles when the particle is moving along the *y*-direction, the configuration shown in Fig. 2(a) is used here too. The separation distance between the microcylinder and nanoparticle is 40 nm in *x*-direction and the diameter of the silver nanoparticle is 120 nm. The wavelength is 400 nm. The fields are monitored on the x axis at a distance of 2.1 μm from the surface of the microcylinder; (b) The optically induced force for *H*-polarization [same configuration as in Fig. 2(a)].

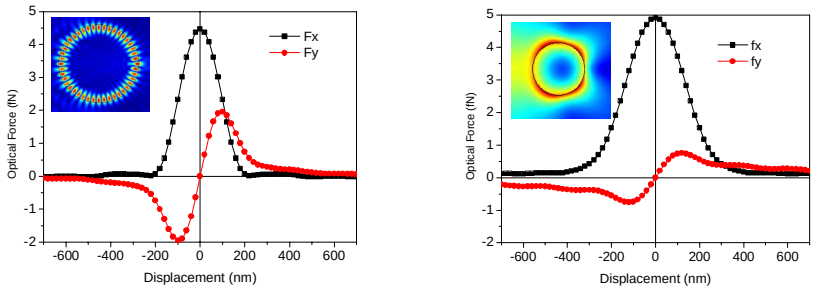

(a) (b)

Fig. 7. Calculation of the optically induced force under resonance conditions. (a) For *E*-polarization; the resonance wavelength of the microcylinder is 383nm. Inset: electric field (*Ez* component) distribution of the WGM. (b) For *H*-polarization; the resonance wavelength of the nanoparticle is 350nm. Inset: electric field distribution of the metallic nanoparticle at 350nm.

Recent studies have shown that the optically induced forces between coupled metal nano-particles can be enhanced when the particles are driven at resonance [14]. We will therefore focus on force calculations at both resonances, namely of the microcylinder and of the nanoparticle. The configuration in Fig. 2(a) is used again for the data displayed in Fig. 7. One of the resonances of the microcylinder under *E*-polarization was chosen (i.e., at 383 nm), with an electric field distribution (*Ez* component) as shown in the inset of Fig. 7(a), which represents a WGM with mode number $m = 1$ and $n = 22$. Close to this resonance, most of the incident field is captured by the microcylinder, and the PNJ is absent. When a nanoparticle is transgressing the area that would be occupied by a potential PNJ, the WGM is still present but with a significantly enhanced amplitude. This means that due to the presence of the nanoparticle more electromagnetic energy is reflected back into the microcylinder. Another explanation may refer to the nanoparticle's evanescent scattering components, which provides a reactive tuning mechanism for a more pronounced reproduction of the WGM mode. The optical force shown in Fig. 7(a) is larger than for the non-resonant case [e.g., Fig. 2(b)]. We attribute the enhancement of the optical force to the large gradient of the evanescent field of the WGM in the microcylinder. However, it should be noted that plane wave illumination is

#98001 - $15.00 USD Received 30 Jun 2008; revised 14 Aug 2008; accepted 15 Aug 2008; published 19 Aug 2008

not the most efficient way to excite the WGM in the microcylinder, since most of the light is coupled to non-resonant, dissipative modes. Figure 7(b) shows the optical force acting on the particle when it operates on the single resonance of the particle at 350 nm under *H*-polarization. As can be seen in Fig.7, the amplitude of *fx* in Fig. 7(b) is larger than that of *fx* in Fig. 7(a); while the amplitude of *fy* is decreased when the PNJ is present [Fig. 7(b)]. This indicates that the forces (e.g. *fy*) can be tailored in some sense, i.e., when one compared the PNJ induced force with the WGM induced force. We can therefore manipulate nanoparticles efficiently by using the features of PNJ induced forces. The enhanced optical forces are attributed to the increased SCS of nanoparticle at resonance, which essentially originates from the generation of a surface plasmon.

4. Summary

We have analyzed the optically induced forces exerted on a metallic nanoparticle when the nanoparticle is immersed into a PNJ, which is generated by plane wave illumination of a dielectric microcylinder under different polarizations. Resonant and non-resonant wavelengths of the single microcylinder and the nanoparticle were investigated in order to get a better insight into the generation of optically induced forces in such nano configuration. The WGM can be generated in the microcylinder even when the microcylinder is not exactly at resonance, provided that the scattering from the nanoparticle is strong enough. The optical forces are enhanced when the configuration is operated at resonance either of the mircocylinder or of the nanoparticle. The optical forces are strongly affected by the separation distance, the size of the particle, and the wavelength. For small particle sizes together with small separation distances, one has to select the wavelength carefully in order to obtain the desired optical forces. We also showed that the repulsive force could be changed to an attractive force by simply choosing a corresponding polarization of the incident beam. These findings are attractive because PNJs may bridge the gap between a conventional microtechnological environment and e.g. a functional nanodevice, meaning that the generation of PNJ is based on a considerably large object which provides highly confined force fields to efficiently organize nanostructures in the nanoscale.

#98001 - $15.00 USD Received 30 Jun 2008; revised 14 Aug 2008; accepted 15 Aug 2008; published 19 Aug 2008